COBEM 2023 27TH INTERNATIONAL CONGRESS OF MECHANICAL ENGENEERING

ABCM Brazilian Society of Mechanical Sciences and Engineering
27th ABCM International Congress of Mechanical Engineering
December 04-08, 2023, Florianópolis-SC, Brazil

COB-2023-2381
DISTANCE-TO-TRAP WEIGHTING FUNCTIONS FOR SELECTION AND RANKING OF CO_2 STORAGE SITES

José Wilker de Lima Silva
TRIL Lab, Federal University of Paraíba, João Pessoa, Brazil
State University of Paraíba, João Pessoa, Brazil
wilker@servidor.uepb.edu.br

Moisés Dantas dos Santos
Gustavo Charles Peixoto de Oliveira
TRIL Lab, Federal University of Paraíba, João Pessoa, Brazil
mdantas@ci.ufpb.br, gustavo.oliveira@ci.ufpb.br

Abstract. *Several countries are boldly committed to reaching a carbon neutrality scenario by 2050. Geologic carbon storage (GCS) is a bridging technology under the broader carbon capture, utilization, and storage (CCUS) scope that now spearheads the Net Zero race. The goal of the CCUS chain is to capture the carbon dioxide (CO_2) dispersed into the atmosphere, recycle it for further usage, or transport it to suitable locations through a pipeline network, and finally inject it into deep geological formations for permanent storage. Regardless of numerous GCS projects that have succeeded around the globe mainly fostered by the oil and gas industry, the reality of full-scale GCS projects still is very young in Brazil. So far, there is only one CCUS operational project in the country, currently located in Santos Basin and totally devoted to enhanced oil recovery. The database of storage, injectivity, and containment mechanisms of CO_2 in potential storage sites, like saline aquifers and depleted reservoirs, is also limited. This paper intends to present a few mathematical models for qualifying potential underground CO_2 storage sites. We studied a group of functionals endowed with distinct weighting functions with two main objectives. First, to explain the nonlinear relationship of rock and fluid properties through rock quality estimates. Second, to grade field regions taking into account multiple structural traps featured by caprocks. The method works as a suggestive resource for convenient injection and storage loci. We implemented the models computationally through the Matlab Reservoir Simulation Toolbox (MRST) software and organized a case study over the UNISIM-I-D model, a representation of the Namorado Field (Campos Basin, Brazil). Preliminary results show that, decaying exponential, logistic or hybrid functions can lead to different storage sites, locations for injection wells, and storage surpluses. In contrast to the injection performance of in-field legacy wells, our approach reaches modest gains. The ultimate purpose of this study is to provide a knowledge base for future GCS projects in Brazil.*

Keywords: *Carbon neutrality, geologic carbon storage, computational methods, reservoir characterization.*

1. INTRODUCTION

The increasing global energy demand has compelled society and public entities to explore mechanisms aimed at reducing carbon dioxide emissions into the atmosphere, as it is the primary driver of anthropogenic climate change (Stocker, 2014; Rose *et al.*, 2017; Cook *et al.*, 2016; Verheggen *et al.*, 2014). Such transitional move towards a carbon-neutral state, known as Net Zero, is being anticipated by a gradual decline in energy production from fossil fuel sources, without, however, compromising the energy supply (Bouckaert *et al.*, 2021).

As the world strives to establish a sustainable energy framework, carbon capture and storage (CCS) has emerged as a bridging technology for mitigating CO_2 emissions and, consequently, greenhouse gases. While this technique first appeared in the literature during the 1970s, it gained substantial attention only two decades later. The fundamental concept turns around capturing the CO_2 generated by industrial processes involving fuel combustion, transporting it to suitable locations, and injecting it into deep geological formations for permanent storage, thereby preventing its release into the atmosphere (Agency, 2016; Godec *et al.*, 2011; Bruhn *et al.*, 2016; Rogelj *et al.*, 2016).

Since the mid-1990s, the underground injection of CO_2 has been primarily implemented within the oil and gas sector, so featuring a branch termed *geological carbon storage* (GCS). Nevertheless, numerous challenges persist for GCS to become a fully integrated and commercially viable technology. Careful evaluation of storage locations is also crucial. Typically, geological formations such as depleted oil and natural gas reservoirs, inactive coal deposits, and aquifers with substantial storage capacity and long-term security are considered suitable choices. Recent studies have emphasized that the major areas of interest for GCS in Brazil extend from North to South, both onshore and offshore, but their individual storage capacity varies dramatically (Figure 1).

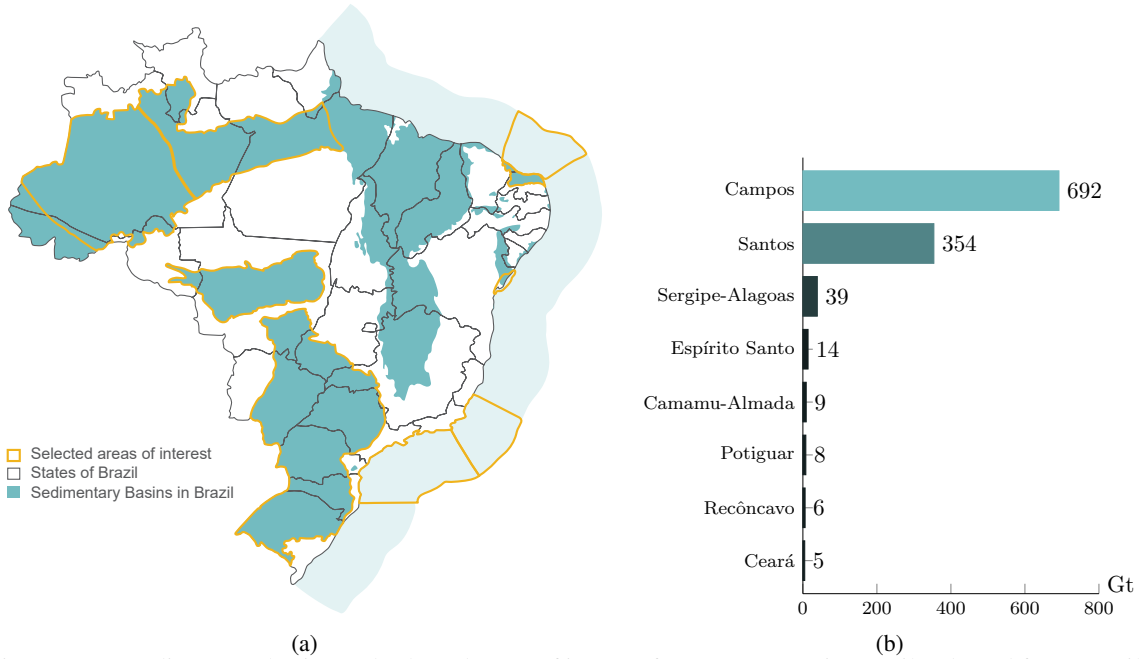

(a) (b)

Figure 1: (a) Sedimentary basins and selected areas of interest for CO_2 storage in Brazil (adapted from Brasil (2023)); (b) Brazilian basins with the largest theoretical storage capacities of supercritical CO_2 in Gigatons (adapted from Ciotta *et al.* (2021)).

The estimated global storage capacity for CO_2 is highly associated to depleted gas reservoirs (Ladbrook *et al.*, 2009) whose total capacity is roughly ten times the annual rate of CO_2 emissions worldwide. However, Harding *et al.* (2018) state that up to 90% of the injected gas can escape the storage site over a period of 2000 years, with an annual leakage rate of 0.1%. In Brazil, the storage potential is estimated to be larger than 2035 Gt (Iglesias *et al.*, 2015; Drexler *et al.*, 2020; Ciotta *et al.*, 2021).

To ensure a return on investment, it is crucial to keep the CO_2 securely trapped within the rock formations. Leakage, even at a slow rate, over an extended period can undermine the entire project. Even a modest loss of 0.1% of the storage's inventory each year renders it ineffective and potentially hazardous. Therefore, ensuring the integrity of GCS projects is of paramount importance. Aiming to address these concerns and challenges, this paper proposes a comprehensive study of qualifying functionals, which are compounds of underlying functions focused on identifying suitable injection sites and predicting the paths of the gas plume. This process, defined as site qualification, is dedicated to constructing measurable criteria both mathematically and geologically consistent applicable to site characterization of future GCS ventures in Brazil.

2. METHODOLOGY

2.1 Flow deliverability potential

Reservoir quality index (RQI) is a widely known technique to assess the quality of reservoirs formerly defined as a function of the reservoir process speed, namely the permeability-to-porosity ratio (Amaefule *et al.*, 1993). By using averaging, the form

$$RQI = 0.0314\sqrt{\frac{\kappa}{\phi}} \quad [\mathrm{m}^2], \quad \text{with } \kappa = \sqrt{k_x^2 + k_y^2 + k_z^2} \quad [\mathrm{m}^2], \tag{1}$$

where κ and ϕ are the average permeability and porosity, in this order, and 0.0314 is a unit conversion from millidarcies, is recently featured as the appropriate parameter for characterizing petrophysical dynamic flow units (Mirzaei-Paiaman *et al.*, 2018, 2019; Mirzaei-Paiaman and Ghanbarian, 2022). For our purposes, Eq. (1) is termed the *flow deliverability potential function*.

2.2 Reservoir model and trap analysis

To test the current approach for well placement, we considered a reduced version of the UNISIM-I-D model, representative of the Namorado field, located in Campos Basin, Brazil (Avansi and Schiozer, 2015). Th reduced model has 8083 active cells, average pore volume of around $1.33 \times 10^4\ \mathrm{m}^3$, and maximum porosity of 0.3. The discrete version of

the reservoir is described by

$$\Omega = \{c_{(i,j,k)}; 1 \leq i \leq I,\ 1 \leq j \leq J,\ 1 \leq k \leq K\},\ \ I, J, K \in \mathbb{Z}_+^*, \tag{2}$$

which denotes the 3D logical indexing of cells c in a corner-point grid. By applying the trap analysis resource available in `MRST-co2lab` module, it is possible to visualize how spill paths, spill points, catchment regions, and traps are all hierarchically interconnected by "rivers" (Nilsen *et al.*, 2015). The trap analysis over the reduced model looks like a "spider"-like network of 11 traps (Figure 2) and total storage capacity of around $1.6 \times 10^7\ \mathrm{m}^3$.

(a) 3D view (b) Top view

Figure 2: Traps and rivers network of the reduced UNISIM model. When CO_2 begins to escape from a given trap, it migrates upwards until it reaches the next one through connected paths called "rivers". Traps with smaller capacities interspersed in the network are called subtraps and the core trap at the center of the model has the largest storage capacity.

2.3 Distance-to-trap functions

To locally weigh the quality of a storage site, distances are an effective way for assigning degrees of relevance to locations in the surroundings of a trap. By taking reference points inside a trap, we constructed distance-to-trap functions, or β-functions, that qualify all reservoir grid cells in the range (0,1] in relation to their relative position to all traps. In this paper, we study how the functionals are altered when subject to one of the following β-functions:

$$\beta_1(c) \ = \ \underset{1\leq\tau\leq n_\tau}{\text{mean}}\ \{\beta_{1,\tau}(c)\}, \tag{3a}$$

$$\beta_2(c) \ = \ \underset{1\leq\tau\leq n_\tau}{\text{mean}}\ \{\beta_{2,\tau}(c)\}, \quad \text{and} \tag{3b}$$

$$\beta_3(c) \ = \ \underset{1\leq\tau\leq n_\tau}{\text{mean}}\ \{\beta_{3,\tau}(c)\}, \tag{3c}$$

with

$$\beta_{1,\tau}(c) \ = \ \begin{cases} 1, & \text{if} \quad 0 < d_1(\tau) \leq 1, \\ \{\log[d_1(\tau)]\}^{-1}, & \text{otherwise} \end{cases} \tag{4a}$$

$$\beta_{2,\tau}(c) \ = \ -\frac{1}{1 + \frac{1}{\upsilon}\exp\Big[-\Big(\frac{d_1(\tau) - d_2(\tau)}{n_\mathcal{T}}\Big)\Big]} \tag{4b}$$

$$\beta_{3,\tau}(c) \ = \ \exp\Big[-\frac{d_1(\tau)}{d_3(\tau)}\Big], \tag{4c}$$

for $\tau = 1, 2, \ldots, 11$. Above, $d_1(\tau)$ is the distance from the centroid of the cell c to the top of the trap τ, $d_2(\tau)$ is the maximum distance among all distances from the trap's top projection onto the spill point plane to the trap's boundary, $d_3(\tau)$ is the maximum distance among all distances from the trap's top to the field's boundary, and $n_\mathcal{T}$ is the number of traps. Since the injectable gaseous mass is limited by the effective trap capacity, it is appropriate to define the *trap volume ratio* as $\upsilon = \frac{\text{vol}(\mathcal{T})}{\text{vol}(\mathcal{T}^c)}$, where vol stands for "volume" and $\mathcal{T}^c$) is the catchment region of a trap excluding the own trap region. One expects that $\upsilon < 1$ because the effective trap volume usually is higher than the transitional region volume.

Graphically, β_1 has a short plateau near the trap's top inside the trap domain that precedes a soft decay that extends until the "dead zone" (region where the β function vanishes asymptotically), β_2 is a logistic function, featured by an abrupt change at the interface between the catchment region and the "dead zone", and β_3 is a hybrid logistic function with monotonic decay (Figure 3).

2.4 Qualifying functionals

A qualifying functional is a function of other underlying functions whose composition may depend on many variables. For our purposes, the 3D space (discretely represented by all grid cell centroids c) is the running variable and time is fixed

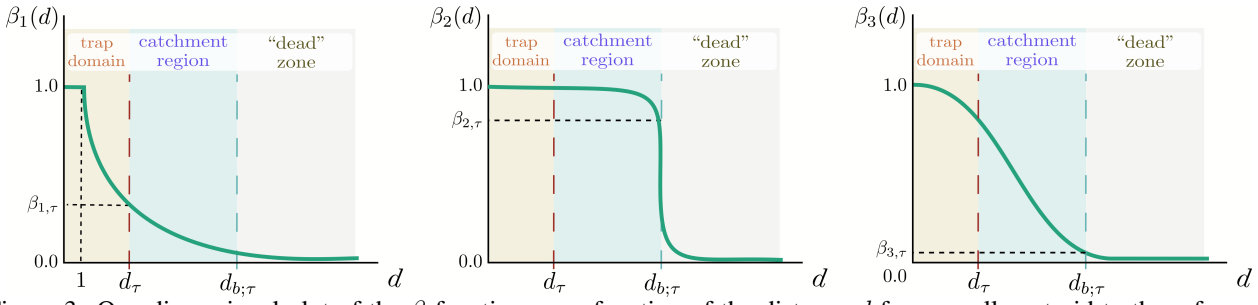

Figure 3: One-dimensional plot of the β functions as a function of the distance d from a cell centroid to the reference points determined by Equations (3a-3c).

at a initial state ($t = t_0$). The role of a functional is assess how much a reservoir site is adequate for storage. Beyond the flow deliverability function defined in Eq. (1) and the distance-to-trap functions defined in Eqs. (3a - 3c), other usual quantities are admissible as underlying functions. This way, the qualifying functionals proposed for analysis are combined so resulting in a family of seven members:

$$J_1(c,t) = \phi(c)\kappa(c)s_w(c,t), \tag{5a}$$
$$J_2(c,t) = J_1\beta_1(c), \tag{5b}$$
$$J_3(c,t) = J_1\beta_2(c), \tag{5c}$$
$$J_4(c,t) = J_1\beta_3(c), \tag{5d}$$
$$J_5(c,t) = RQI(c)s_w(c,t)\beta_1(c), \tag{5e}$$
$$J_6(c,t) = RQI(c)s_w(c,t)\beta_2(c), \tag{5f}$$
$$J_7(c,t) = RQI(c)s_w(c,t)\beta_3(c). \tag{5g}$$

Equations (5a-5g) combine static and dynamic properties, although all of them are computed at a fixed instant. Along side RQI, brine saturation s_w and the β-functions create a compound of quantities that provide different meanings and interpretations for the functional based on their dimensional units. We adopted the functional of Eq. (5a) as an adapted benchmark (Kharghoria *et al.*, 2003) due to the limited literature for storage purposes. As a final step, the J_i functionals are normalized and made dimensionless through a min-max rule, so that $0 < J_i \leq 1$, $i = 1, \ldots, 7$.

2.5 Discrete dynamic units and injectivity unit classes

The current methodology relies on the concept of discrete dynamic units (DDUs). A DDU is a rock with similar fluid flow behavior experimental proved to have superior dynamic quality grounded on the flow deliverability potential (Mirzaei-Paiaman *et al.*, 2018, 2019). From the discrete point of view, DDUs are cells of the computational grid connected by similar values of a functional J (Figure 4).

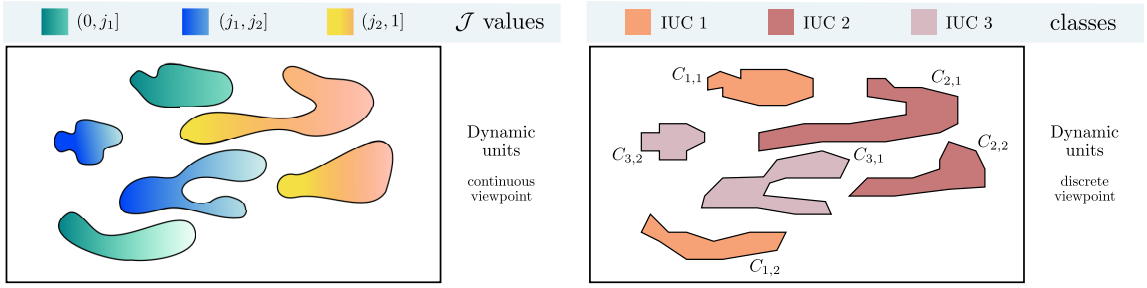

Figure 4: Representation of dynamic units in continuous and discrete viewpoints. The $C_{D,q}$ notation is introduced in Eq. (7).

The DDUs are converted into injectivity unit classes (IUCs) by a procedure previously applied for production tests (Oliveira *et al.*, 2020a,b, 2021). To an IUC is ascribed a unique positive integer value that may encompass different dynamic units. The approach used to classify dynamic units applies a binning method B which computes the number of IUCs, the class range, and class partitions of J over all grid cells, making a continuous-to-discrete transform (Figure 5) by the transform given by

$$\mathrm{IUC}(c) = B(J(c)), \quad \forall c \in \overline{\Omega}. \tag{6}$$

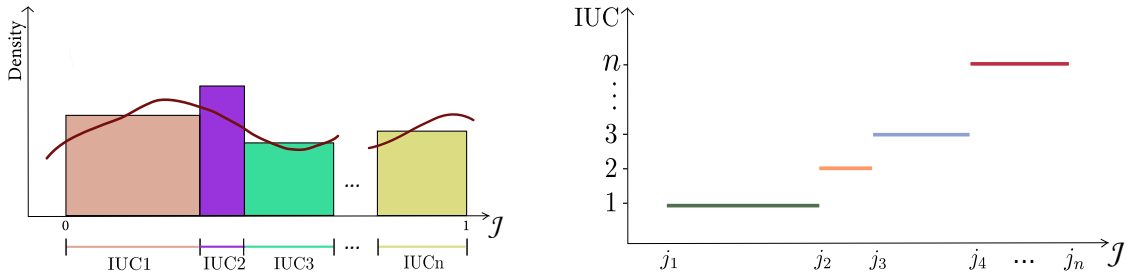

(a) Histogram of injectivity unit classes (IUCs) overlaid by a density curve model.

(b) Integer function resulting from the binning transform.

Figure 5: Binning transform procedure from a functional J to injectivity classes.

Equation (6) represents a classifier function that will generate up to N finite classes. It is desirable that N is small so that the number of injection sites do not overburden the numerical simulations. We have applied four binning methods from known algorithms to provide enough explainability of the distribution: `scott` (Scott, 2015), `freedman-diaconis` (Freedman and Diaconis, 1981), `sturges` (Sturges, 1926), and `sqrt` (Davies *et al.*, 1947).

2.6 Storage sites and injection well placement

Once computed, the DDUs become identifiable as smaller storages (clusters) defined by

$$C_{D,q} := \{c;\ IUC(c) = D \ \text{ and } c \in N_6(c_s)\}, \tag{7}$$

where $q = 1, 2, \ldots, Q$ is the cluster index, c_s is the central cell, and N_6 is a 6-neighbor face-connected aggregator used to produce connectivity among cells belonging to the same IUC. Each cluster can comprise a distinct number of interconnected cells, represented by n_q. Consequently, $C_{D,q}$ represents either a constituent portion of or an entire DDU.

We associated the storage $C_{D,q}$ to a graph $G_{D,q}$ through a one-to-one function $\mathcal{G}$ that maps a cell of the storage onto a node of the graph (Figure 6).

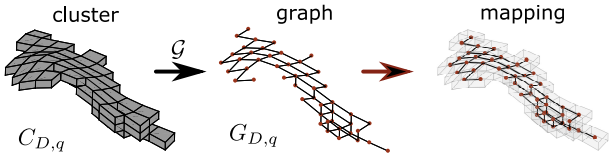

Figure 6: Cluster-to-graph mapping for a storage site: $C_{D,q}$ is a cluster formed by face-connected grid cells mapped onto nodes of a graph $G_{D,q}$. Source: Oliveira *et al.* (2021).

As with the clusters are used to model a volumetric injection site, we employed the metric known as *closeness centrality* to determine the exact injection well placement. The closeness centrality of each node $v_q \in G_{D,q}$ is computed as

$$\gamma(v_q) = \frac{1}{\sum_{i=1}^{\eta_\lambda} d(v_q, v_n)}, \ \forall v_n \in G_{D,q},\ v_n \neq v_q, \tag{8}$$

where $d(v_q, v_n)$ is the shortest path distance between v_q and v_n (Freeman, 1978; Newman, 2010).

However, since the γ values change per node, we computed the *maximum closeness centrality* (MCC) of the cluster $C_{D,q}$ to determine a single well placement locus that matches the bottom hole point (Figure 7).

2.6.1 Hierarchy and intersections

We consider a 4-indices hierarchical tree of elements (J, B, D, q) to represent potential storage sites, where $J = \{1, \ldots, 7\}$, $B = \{1, 2, 3, 4\}$ enumerates the functionals, B the binning methods (`scott`=1, `fd`=2, `sturges`=3, `sqrt`=4), D the IUCs, and q the cluster indices. This way, any element of the tree is completely determined by the functional and the binning method, since the classes and clusters are consequential (Figure 8).

However, it is possible that two or more elements share the same field region due to overlaps of the statistical distributions (Figure 8a. Then, these intersecting storage sites must be eliminated. To this end, we considered that two elements are homologous if their Jaccard index relative to the number of sharing grid cells exceeds the threshold of 75% (3rd quartile) of the distribution of paired elements.

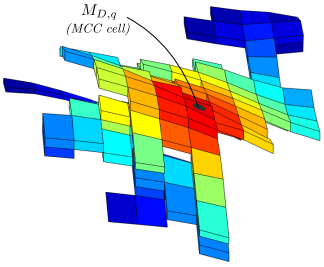

Figure 7: Closeness centrality (γ) distribution over a hypothetical cluster. It varies from lower values (colder colors) to higher values (hotter colors) within the unit interval. The black dot indicates the maximum closeness centrality cell ($M_{D,q}$).

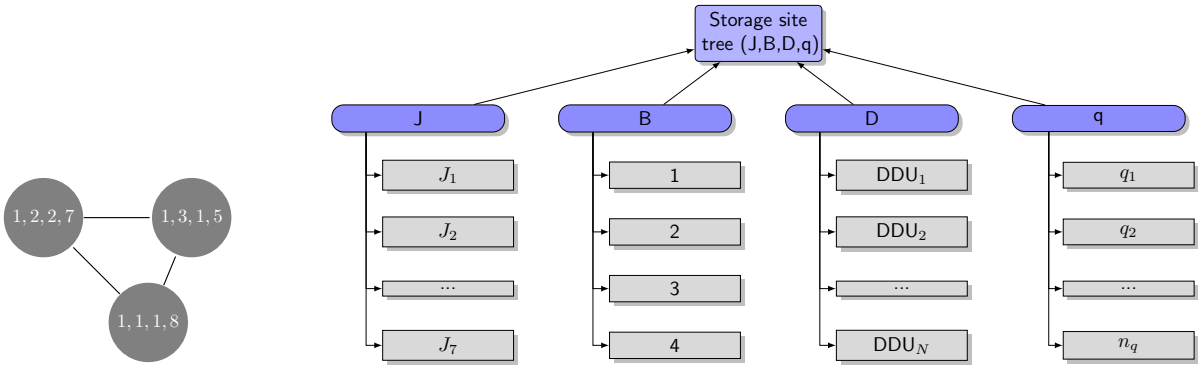

(a) (b)

Figure 8: Storage site organization: (a) example of three intersecting instances, where the elements (1,2,2,7) and (1,3,1,5) are homologous to (1,1,1,8); (b) hierarchical tree of functionals, binning methods, IUCs and cluster indices.

Originally, the Jaccard index measures the similarity between finite sets of samples. Also termed intersection-over-union ratio, it is defined here as (Agresti, 2012):

$$\text{Jacc}(S_1, S_2) = \frac{\#(S_1 \cap S_2)}{\#(S_1 \cup S_2)}, \tag{9}$$

where the numerator is the number of grid cells of the intersection region between the storage sites S_1 and S_2, and the denominator the number of grid cells of their union. Naturally, $0 \leq \text{Jacc}(S_1, S_2) \leq 1$. When $Jacc \geq Jacc^* = 0.75$, all circular dependence between intersecting pairs are eliminated and the number of storage sites subject to simulations may reduce considerably.

2.7 Fluid flow model

The dynamics of CO_2 injection and migration can be modeled using two components, brine (w) and gas (g), which coexist in the porous medium as aqueous and supercritical phases, respectively, under aquifer conditions (Nilsen *et al.*, 2017). In turn, the fluid flow model reads as a two-phase version of the mass conservation equation for a porous medium, i.e.

$$\frac{\partial(\phi\rho_\alpha s_\alpha)}{\partial t} + \nabla \cdot \rho_\alpha \mathbf{u}_\alpha = \rho_\alpha q_\alpha, \quad \alpha = w, g, \tag{10}$$

under the assumption of Darcy's flow for the velocity field

$$\mathbf{u}_\alpha = \kappa\lambda_\alpha(\nabla p_\alpha - \rho_\alpha \mathbf{g}), \tag{11}$$

where ρ is the density, q is the volumetric flux resulting from sources or sinks, α indicates the fluid, λ is the fluid mobility, dependent on the relative permeability and fluid viscosity, p is the pressure, and $\mathbf{g}$ is the gravitational acceleration. Additionally, the following relations for saturations, fluid mobility and capillary pressure p_c as functions of the water saturation close the required equations

$$s_w = 1 - s_g, \tag{12a}$$
$$\lambda_\alpha = \lambda_\alpha(s_w), \tag{12b}$$
$$p_c = p_n - p_w = P_c(s_w). \tag{12c}$$

The system represented by Eqs. (10-12c) is solved for 3D under a vertical equilibrium (VE) assumption that ensures computational efficiency and reasonable physical approximations for CO_2 injection into large aquifers (Nilsen *et al.*, 2017). For the VE formulation, each quantity is replaced by its vertically-averaged counterpart (Nilsen *et al.*, 2011; Bandilla *et al.*, 2014; Nilsen *et al.*, 2016).

3. RESULTS AND DISCUSSION

3.1 Numerical simulations

To carry out numerical simulations of CO_2 injection over the potential storage sites obtained from the hierarcical tree after the $Jacc^*$ thresholding, the `MRST-co2lab` simulator setup was prepared for representing rock-fluid properties and numerical parameters consistent with the literature (Table 1). The injection well placement over each storage site matches the MCC cell determined by Eq. (8), in which a single well is allocated to operate and pump the gas into the formation.

Table 1: Simulation setup used in `MRST-co2lab` for all numerical experiments.

Parameter	**Value**
Residual brine saturation	0.11
Residual CO_2 saturation	0.21
Brine viscosity	0.3086 cP
CO_2 viscosity	0.0566 cP
Brine density	975.86 $\mathrm{kg/m^3}$
CO_2 density	686.54 $\mathrm{kg/m^3}$
Brine relative permeability	0.2142
CO_2 relative permeability	0.8500
Gravity acceleration	9.8066 $\mathrm{m/s^2}$
CO_2 injection rate	$10.22 \cdot 10^6$ $\mathrm{m^3/year}$
Injection time span	100 years
Migration time span	1900 years
Average well bottomhole depth	3090 m

3.1.1 Comparative CO_2 storage inventory

The methodology explained so far produced 7 best locations for placement of the injection wells, resulting in the following sets of storage sites (elements of the hierarchical tree):

$$\mathcal{S}_{J=\{2-4\}} = \{(2,1,1,6),\,(3,1,3,2),\,(4,1,1,6)\} \tag{13}$$

$$\mathcal{S}_{J=\{5-7\}} = \{(5,1,27,1),\,(6,1,5,5),\,(7,1,22,2)\}, \tag{14}$$

according to their respective functionals. For purposes of benchmarking, we considered two other sets:

$$\mathcal{S}_{J=1} = \{(1,1,1,8)\} \quad \text{(analytic benchmark)} \tag{15}$$

$$\mathcal{S}_{legacy} = \{NA2,\, RJS19,\, NA1A,\, NA3D\} \quad \text{(physical benchmark)}. \tag{16}$$

$\mathcal{S}_{J=1}$ relates to wells based on an analytic approach adapted from Kharghoria *et al.* (2003), whereas $\mathcal{S}_{legacy}$ includes legacy wells experimentally existing in the field. Analogously, we denoted by $W_{j,b,d,q}$ the injection well associated to the element (j,b,d,q). In turn, we compared the injection performance for the best 11 wells associated to the sets of Eqs. (13-16) based on the post-selection of previous testing simulations (Table 2). The CO_2 inventory comprises 6 categories, among which only the total residual is used for analysis (Table 3).

3.1.2 CO_2 dynamics and injected mass

The dynamics of the inventory states can be viewed through a time vs. injected mass plot in which the colored areas represent proportions of the total mass of CO_2 injected into a specific storage site (Figure 9). All cases simulated have a similar dynamics due to the shareable numerical setup. Initially, a fast and steep change in mass emerges as a response to the continuous injection process that lasts for 100 years. Next, during the post-injection stage, one observes the outset of plateaus for the residual storage or leakage that extend over 1900 years, or asymptotic behavior representing how CO_2 migrates slowly inside the formation (Figure 10).

Table 2: Percentual distribution of total injected volume. Wells with best residual trapping are highlighted in bold.

J, B, D, q	Resid. (traps)	Resid.	Resid. (plume)	Total Resid.	Mov. (traps)	Mov. (plume)	Leaked
$5, 1, 27, 1$	5.52	31.58	10.45	**47.56**	17.87	33.84	0.73
$7, 1, 22, 2$	5.52	31.43	10.57	**47.52**	17.87	34.23	0.37
$6, 1, 5, 5$	5.52	31.87	10.00	**47.39**	17.87	32.37	2.37
$3, 1, 3, 2$	5.52	31.05	10.71	**47.28**	17.87	34.68	0.17
$2, 1, 1, 6$	5.52	30.16	10.88	**46.57**	17.87	35.25	0.31
$4, 1, 1, 6$	5.52	30.16	10.88	**46.57**	17.87	35.25	0.31
$1, 1, 1, 8$	5.52	30.16	10.88	**46.57**	17.87	35.25	0.31
NA2	5.53	25.72	12.00	**43.24**	17.89	38.86	0.00
RJS19	4.96	20.62	13.38	**38.96**	16.05	43.33	1.66
NA1A	4.94	16.92	14.67	**36.52**	15.98	47.50	0.00
NA3D	4.92	14.09	7.71	**26.72**	15.94	24.96	32.38

Table 3: Default CO_2 storage inventory states and their description according to the `MRST-co2lab` module.

State	Description	Color
Structural residual (R_1)	CO_2 both residually and structurally trapped	
Residual (R_2)	CO_2 residually (but not structurally) trapped, outside the free-flowing zone	
Residual in plume (R_3)	CO_2 still inside the free-flowing zone residually (but not structurally) trapped	
Structural plume (SP)	CO_2 structurally (but not residually) trapped	
Free plume (FP)	CO_2 neither structurally nor residually trapped	
Leaked (L)	CO_2 escaped outward the simulated domain	

3.2 Discussion

The family of functionals introduced here comprises different levels of complexity in terms of their constituent properties. In contrast to the analytic benchmark J_1, three other functionals (J_2, J_3, and J_4) were created as direct derivation by embodying the β-functions and having associated to them the set $\mathcal{S}_{J=2-4}$ of storage sites. The performance of the wells $W_{3,1,3,2}$, $W_{2,1,1,6}$, and $W_{4,1,1,6}$ in terms of residual storage was 47.28%, 46.57%, and 46.57%. The second group of functionals compared under the analytic viewpoint coupled the RQI (J_5, J_6, and J_7) as an alternative to the qualification of the storage sites. Moreover, the β-functions were added in the same manner by producing the set $\mathcal{S}_{J=5-7}$. In this case, the performance of the wells $W_{5,1,27,1}$, $W_{7,1,22,2}$, and $W_{6,1,5,5}$ in terms of residual storage was 47.56%, 47.52%, and 47.39%. In contrast, the performance of the four legacy wells $NA2$, $RJS19$, $NA1A$, and $NA3D$ in terms of residual storage was 43.24%, 38.96%, 36.52, and 26.72%.

From these outcomes, we can draw the following comments:

- Out of six best wells proposed by the current approach (excluding the analytic benchmark well), four overcame the analytic benchmark, namely $W_{5,1,27,1}$, $W_{7,1,22,2}$, $W_{6,1,5,5}$, and $W_{3,1,3,2}$. This implies that the approaches considering the RQI deliver superior qualification power for storage site selection and that the order of increasing performance of the distance-to-trap functions is β_1 followed by β_3, then β_2.

- A reason why $W_{2,1,1,6}$ and $W_{4,1,1,6}$ gave identical results to the analytic benchmark is due to possible matches of MCC cells falling on the 25% remnant portion of the overlapping sites not captured by the Jaccard filtering. As a consequence, the well placement algorithm assigns the same cell positions for injection.

- The set $\mathcal{S}_{legacy}$, which represents legacy producing wells that could be converted to injecting wells and harnessed for CO_2 storage, presented inferior performance and high leakage. In particular, for $NA3D$, the total residual gas stored reached a limit of 26.72%, whereas the leakage was 32.38%.

- While it is clear that the β functions had a positive effect upon the benchmark functional J_1, the relative surpluses were below 1% due to modeling factors, such as fixed brine saturation and small variations of pressure. This modest gain is, however, an indication that the functionals improve the site qualification and have usability for the industry. Based on the current study case, it is not clear which functional must occupy the first rank because their performance

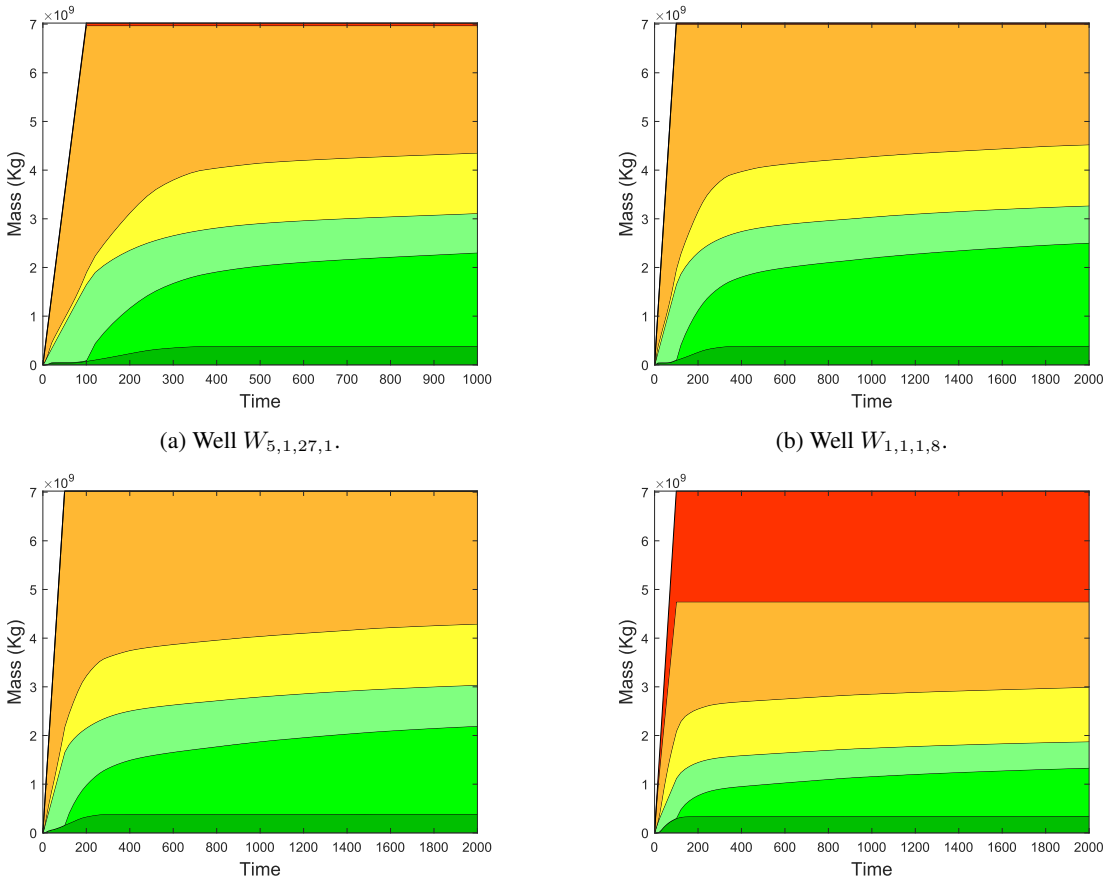

(a) Well $W_{5,1,27,1}$.

(b) Well $W_{1,1,1,8}$.

(c) Well $NA2$.

(d) Well $NA3D$.

Figure 9: Total CO_2 mass injected over time and storage dynamics for four sampled wells. The colored areas represent proportions of a given inventory site as described in Table 3. The time frame considers 100 years of uninterrupted injection and 1900 years of migration.

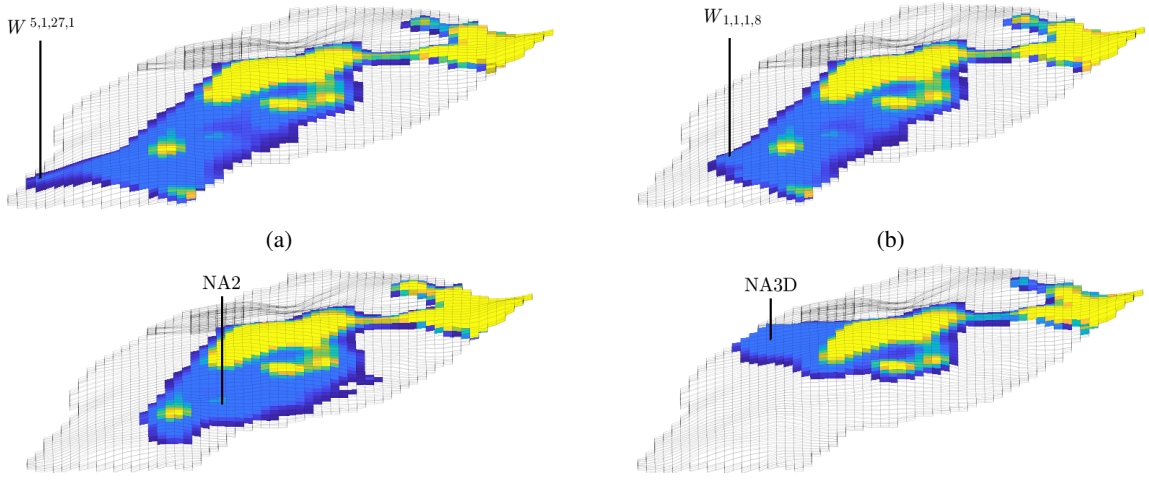

(a)

(b)

(c)

(d)

Figure 10: Numerical simulations of injection for the cases of Figure 9. The plots display the CO_2 saturation at a time instant of 1000 years post-injection. (a) Well $W_{5,1,27,1}$; (b) Well $W_{1,1,1,8}$; (c) Well $NA2$; (d) Well $NA3D$.

is tightly competitive. However, it is undeniable that the incorporation of parameters related to the traps into the β-functions place functionals like J_5 and J_7 at the top of the best performances.

4. CONCLUSION

This paper examined a family of qualifying functionals that combined injectivity unit classes and parameters based on distance-to-trap weighting functions as an alternative to define appropriate CO_2 injection sites. On its track to support site selection workflows, our results showed that the functionals equipped with the flow deliverability function produced higher CO_2 residual storage.

The distance-to trap functions have a complementary role as underlying elements of the functionals, although their individual effect on the site qualification is hard to measure because of the inherent nonlinearity of the functions. On the other hand, one verified that β_1 and β_2 disputed for the top ranks.

To expand this study, further investigation on the effect of the β-functions for the qualifying functionals is necessary, as with the participation of the other functions under larger variations. This gap can be filled in through the inclusion of time-varying quantities especially by geomechanical coupling.

5. REFERENCES

Agency, I.E., 2016. *20 years of carbon capture and storage: Accelerating future deployment*. International Energy Agency.

Agresti, A., 2012. *Categorical data analysis*, Vol. 792. John Wiley & Sons.

Amaefule, J.O., Altunbay, M., Tiab, D., Kersey, D.G. and Keelan, D.K., 1993. "Enhanced reservoir description: using core and log data to identify hydraulic (flow) units and predict permeability in uncored intervals/wells". In *SPE annual technical conference and exhibition*. OnePetro.

Avansi, G.D. and Schiozer, D.J., 2015. "Unisim-i: synthetic model for reservoir development and management applications". *International Journal of Modeling and Simulation for the Petroleum Industry*, Vol. 9, No. 1, pp. 21–30.

Bandilla, K.W., Celia, M.A. and Leister, E., 2014. "Impact of model complexity on co2 plume modeling at sleipner". *Energy Procedia*, Vol. 63, pp. 3405–3415.

Bouckaert, S. *et al.*, 2021. "Net zero by 2050: A roadmap for the global energy sector". *International Energy Agency*.

Brasil, C., 2023. "1st annual ccs: Report in brazil 2022/2023". `https://www.ccsbr.com.br/relatorios-anuais`.

Bruhn, T., Naims, H. and Olfe-Kräutlein, B., 2016. "Separating the debate on co2 utilisation from carbon capture and storage". *Environmental Science & Policy*, Vol. 60, pp. 38–43.

Ciotta, M., Peyerl, D., Zacharias, L.G.L., Fontenelle, A.L., Tassinari, C. and Moretto, E.M., 2021. "Co2 storage potential of offshore oil and gas fields in brazil". *International Journal of Greenhouse Gas Control*, Vol. 112, p. 103492.

Cook, J., Oreskes, N., Doran, P.T., Anderegg, W.R., Verheggen, B., Maibach, E.W., Carlton, J.S., Lewandowsky, S., Skuce, A.G., Green, S.A. *et al.*, 2016. "Consensus on consensus: a synthesis of consensus estimates on human-caused global warming". *Environmental Research Letters*, Vol. 11, No. 4, p. 048002.

Davies, O.L. *et al.*, 1947. "Statistical methods in research and production." *Statistical methods in research and production.*

Drexler, S. *et al.*, 2020. "Impact of rock aging time on the initial wettability of minerals and analogue rocks using pre-salt fluids under reservoir conditions". *Offshore Technology Conference Brasil 2019, OTCB 2019*.

Freedman, D. and Diaconis, P., 1981. "On the histogram as a density estimator: L 2 theory". *Zeitschrift für Wahrscheinlichkeitstheorie und verwandte Gebiete*, Vol. 57, No. 4, pp. 453–476.

Freeman, L., 1978. "Centrality in social networks conceptual clarification". *Social Networks*, Vol. 1, No. 3, p. 215 – 239. ISSN 03788733. doi:10.1016/0378-8733(78)90021-7.

Godec, M., Kuuskraa, V., Van Leeuwen, T., Melzer, L.S. and Wildgust, N., 2011. "Co2 storage in depleted oil fields: The worldwide potential for carbon dioxide enhanced oil recovery". *Energy Procedia*, Vol. 4, pp. 2162–2169.

Harding, F.C., James, A.T. and Robertson, H.E., 2018. "The engineering challenges of co2 storage". *Proceedings of the Institution of Mechanical Engineers, Part A: Journal of Power and Energy*, Vol. 232, No. 1, pp. 17–26.

Iglesias, R.S. *et al.*, 2015. "Carbon capture and geological storage in brazil: an overview". *Greenhouse Gases: Science and Technology*, Vol. 5, No. 2, p. 119 – 130. ISSN 21523878. doi:10.1002/ghg.1476.

Kharghoria, A., Cakici, M., Narayanasamy, R., Kalita, R., Sinha, S. and Jalali, Y., 2003. "Productivity-based method for selection of reservoir drilling target and steering strategy". In *SPE/IADC Middle East Drilling Technology Conference and Exhibition*. OnePetro.

Ladbrook, B., Smith, N., Pershad, H., Harland, K., Slater, S., Holloway, S. and Kirk, K., 2009. "Co2 storage in depleted gas fields". Technical report, IEA Technical Report, 2009.

Mirzaei-Paiaman, A. and Ghanbarian, B., 2022. "A new method for characterizing dynamic reservoir quality: Implications for quality maps in reservoir simulation and rock type classification". *Journal of Petroleum Science and Engineering*, Vol. 218. ISSN 09204105. doi:10.1016/j.petrol.2022.111049.

Mirzaei-Paiaman, A., Ostadhassan, M., Rezaee, R., Saboorian-Jooybari, H. and Chen, Z., 2018. "A new approach in petrophysical rock typing". *Journal of Petroleum Science and Engineering*, Vol. 166, pp. 445–464.

Mirzaei-Paiaman, A., Sabbagh, F., Ostadhassan, M., Shafiei, A., Rezaee, R., Saboorian-Jooybari, H. and Chen, Z., 2019. "A further verification of fzi* and psrti: Newly developed petrophysical rock typing indices". *Journal of Petroleum*

Science and Engineering, Vol. 175, pp. 693–705.

Newman, M., 2010. *Networks: An Introduction*. Oxford University Press, New York.

Nilsen, H.M., Herrera, P.A., Ashraf, M., Ligaarden, I., Iding, M., Hermanrud, C., Lie, K.A., Nordbotten, J.M., Dahle, H.K. and Keilegavlen, E., 2011. "Field-case simulation of co2-plume migration using vertical-equilibrium models". *Energy Procedia*, Vol. 4, pp. 3801–3808.

Nilsen, H.M., Krogstad, S., Andersen, O., Allen, R. and Lie, K.A., 2017. "Using sensitivities and vertical-equilibrium models for parameter estimation of co2 injection models with application to sleipner data". *Energy Procedia*, Vol. 114, pp. 3476–3495.

Nilsen, H.M., Lie, K.A. and Andersen, O., 2016. "Robust simulation of sharp-interface models for fast estimation of co2 trapping capacity in large-scale aquifer systems". *Computational Geosciences*, Vol. 20, No. 1, pp. 93–113.

Nilsen, H.M. *et al.*, 2015. "Spill-point analysis and structural trapping capacity in saline aquifers using mrst-co2lab". *Computers and Geosciences*, Vol. 75, p. 33 – 43. ISSN 00983004. doi:10.1016/j.cageo.2014.11.002.

Oliveira, G., Araújo, E., Santos, M. and Roque, W., 2020a. "Non-uniform injector/producer well pattern designs induced by morphology and anisotropy of flow units". *Journal of Petroleum Science and Engineering*, Vol. 186, p. 106680.

Oliveira, G., Santos, M. and Roemers-Oliveira, E., 2021. "Well placement subclustering within partially oil-saturated flow units". *Journal of Petroleum Science and Engineering*, Vol. 196, p. 107730.

Oliveira, G., Santos, M. and Roque, W., 2020b. "Constrained clustering approaches to identify hydraulic flow units in petroleum reservoirs". *Journal of Petroleum Science and Engineering*, Vol. 186, p. 106732.

Rogelj, J., Den Elzen, M., Höhne, N., Fransen, T., Fekete, H., Winkler, H., Schaeffer, R., Sha, F., Riahi, K. and Meinshausen, M., 2016. "Paris agreement climate proposals need a boost to keep warming well below 2 c". *Nature*, Vol. 534, No. 7609, pp. 631–639.

Rose, S.K., Richels, R., Blanford, G., Rutherford, T. *et al.*, 2017. "The paris agreement and next steps in limiting global warming". *Climatic Change*, Vol. 142, No. 1-2, pp. 255–270.

Scott, D.W., 2015. *Multivariate density estimation: theory, practice, and visualization*. John Wiley & Sons.

Stocker, T., 2014. *Climate change 2013: the physical science basis: Working Group I contribution to the Fifth assessment report of the Intergovernmental Panel on Climate Change*. Cambridge university press.

Sturges, H.A., 1926. "The choice of a class interval". *Journal of the american statistical association*, Vol. 21, No. 153, pp. 65–66.

Verheggen, B., Strengers, B., Cook, J., van Dorland, R., Vringer, K., Peters, J., Visser, H. and Meyer, L., 2014. "Scientists' views about attribution of global warming". *Environmental science and technology*, Vol. 48, No. 16, pp. 8963–8971.

6. RESPONSIBILITY NOTICE

The authors are the only responsible for the printed material included in this paper.